

BLACK HOLE MASSES AND ENRICHMENT OF $Z \sim 6$ SDSS QUASARS¹

JARON D. KURK², FABIAN WALTER

Max–Planck–Institut für Astronomie, Königstuhl 17, D–69117, Heidelberg, Germany

XIAOHUI FAN, LINHUA JIANG

Steward Observatory, The University of Arizona, 933 N. Cherry Avenue, Tucson, AZ 85721

DOMINIK A. RIECHERS, HANS-WALTER RIX

Max–Planck–Institut für Astronomie, Königstuhl 17, D–69117, Heidelberg, Germany

LAURA PENTERICCI

Osservatorio Astronomico di Roma, Via di Frascati 33, I–00040, Monte Porzio Catone, Italy

MICHAEL A. STRAUSS

Department of Astrophysical Sciences, Princeton University, Peyton Hall - Ivy Lane, Princeton, NJ 08544

CHRIS CARILLI

National Radio Astronomy Observatory, PO Box O, Socorro, NM 87801

AND

STEFAN WAGNER

Landessternwarte Heidelberg, Königstuhl 12, D–69117, Heidelberg, Germany

Submitted April 26, 2007 Accepted July 8, 2007

ABSTRACT

We present sensitive near-infrared spectroscopic observations for a sample of five $z \sim 6$ quasars. These quasars are amongst the most distant, currently known quasars in the universe. The spectra have been obtained using ISAAC at the VLT and include the C IV, Mg II and Fe II lines, which are powerful probes of the chemical enrichment and the black hole masses in these objects. We measure the Fe II/Mg II line ratio, as an observational proxy for the Fe/ α element ratio. These elements are produced by different types of supernovae and their abundance ratio can therefore serve as a cosmological clock. We derive a ratio of 2.7 ± 0.8 for our sample, which is similar to that found for lower redshift quasars, i.e., we provide additional evidence for the lack of evolution in the Fe II/Mg II line ratio of quasars up to the highest redshifts. This result demonstrates that the sample quasars must have undergone a major episode of iron enrichment in less than one Gyr and star formation must have commenced at $z \geq 8$. The linewidths of the Mg II and C IV lines give two estimates for the black hole masses. A third estimate is given by assuming that the quasars emit at their Eddington luminosity. The derived masses using these three methods agree well, implying that the quasars are not likely to be strongly lensed. We derive central black hole masses of $0.3 - 5.2 \times 10^9 M_\odot$. These include the lowest black hole mass ever measured at $z \sim 6$, suggesting that we probe a more typical quasar population (with lower masses/luminosities) than examined before. We use the difference between the redshift of Mg II (a proxy for the systemic redshift of the quasar) and the onset of the Gunn Peterson trough to derive the extent of the ionized Strömgren spheres around our target quasars. The derived physical radii are about five Mpc. Using a simple ionization model, the emission of the central quasars would need of order $10^6 - 10^8$ yr to create these cavities in a surrounding intergalactic medium (IGM) with a neutral fraction between 0.1 and 1.0. As the e-folding time scale for the central accreting black hole is on the order of a few times 10^7 years, it can grow by one e-folding or less within this time span.

Subject headings: Galaxies: high-redshift — Galaxies: fundamental parameters — Galaxies: formation — Galaxies: evolution — Quasars: individual: J000552.34-000655.8, J083643.85+005453.3, J103027.10+052455.0, J130608.26+035626.3, J141111.29+121737.4

1. INTRODUCTION

Since the advent of the Sloan Digital Sky Survey (SDSS, York et al. 2000) and other large multi-band surveys, more than twenty quasars at $z \geq 5.7$ have been discovered (mostly by the SDSS: Fan et al. 2000, 2001,

¹ Based on observations carried out at the European Southern Observatory, Paranal, Chile under program Nos. 267.A–5689, 069.B–0289, 071.B–0525, 074.A–0447 and 076.A–0304.

² German Science Foundation’s Collaborative Research Center 439 fellow.

2003, 2004, 2006c, and three in other surveys: Goto 2006; McGreer et al. 2006; Venemans et al. 2007). These quasars provide the best probes of the early growth of supermassive black holes and serve as signposts for overdensities in the universe only one Gyr after the Big Bang. High redshift QSO studies also provide important insight into the reionization (Fan et al. 2006a) of the intergalactic medium (IGM) that took place in the early Universe and into the relation between the formation of early galaxies and black holes (Fan 2006).

Studies of the full SDSS quasar sample from $z = 0$ to $z = 6$ (Richards et al. 2002a; Schneider et al. 2005) show a strong evolution in number density of the quasar phenomenon with redshift (the comoving density of luminous quasars at $z \sim 6$ is about forty times smaller than at $z \sim 3$, Richards et al. 2006c), but there is no evolution detected in the intrinsic spectral properties of these quasar phases (Fan 2006). The high density peaks in the dark matter distribution, which host QSOs, are expected to be much rarer in the early universe (Shen et al. 2007), while the immediate environment of quasars matures apparently very early on. Blueward of the Ly α line, the observed spectra of SDSS quasars do change strongly as a function of redshift, as the absorption by intervening neutral hydrogen increases with redshift up to the point where the continuum emission is completely absorbed (complete Gunn–Peterson (GP) absorption, Gunn & Peterson 1965). The detection of deep GP troughs in 23 $z \sim 6$ QSOs (Fan et al. 2006c) indicates that the IGM is significantly neutral ($n_{\text{HI}}/n_{\text{H}} \sim 10^{-3} - 10^{-2}$) at these redshifts. However, the large dispersion of IGM properties measured along different lines of sight strongly suggests that the reionization process is more complex than a quick phase transition over a narrow redshift range (Fan et al. 2006b). This finding is supported by the results of the Wilkinson Microwave Anisotropy Probe (WMAP, Bennett et al. 2003) mission, which suggest that the universe may have been $\sim 50\%$ neutral at redshift $z \gtrsim 10$, but reionization did not start before $z \sim 14$ (Page et al. 2007). QSOs acting alone cannot have reionized the hydrogen in the IGM prior to $z \sim 4$ (e.g., Meiksin 2005), leaving star-forming galaxies as the most likely candidates to ionize the IGM at $z > 6$.

The strong emission lines excited by the nuclear source of a galaxy can be used to infer various physical and dynamical properties of the circumnuclear gas and therefore its power source, the nuclear black hole. For QSOs at $z > 5.7$, the strong emission lines redward of Ly α are shifted into the near infrared. Several near-infrared (NIR) spectroscopy studies of QSO samples including objects at $z \sim 6$ have been carried out (e.g., Maiolino et al. 2001, 2003; Aoki et al. 2002; Pentericci et al. 2002; Barth et al. 2003; Dietrich et al. 2003; Freudling et al. 2003; Willott et al. 2003; Iwamuro et al. 2004). The results of these early studies show that the Fe II/Mg II line ratio appears to be similar at all redshifts, up to and including $z \sim 6$ (some studies even report higher values than found in the local universe). Assuming that this ratio is directly related to the Fe/ α abundance, this suggests that all observed quasars have undergone a major episode of iron enrichment early on, at least in their nuclear region. We do note one caveat here: at high redshifts, we do not know about the metallicity of less luminous QSOs as, so

far, only the brightest objects have been studied.

The Fe to Mg abundance ratio, and its observational proxy, the Fe II/Mg II line ratio, can be considered a cosmological clock. Both elements are produced in supernova explosions, but while Fe is produced by Type Ia supernovae (SNe), which have relatively low mass progenitors (white dwarfs in binary systems), Mg is produced by Type II SNe, which have high mass progenitors. Mg therefore appears almost instantaneously after initial star formation while the Fe production starts only later. The ratio of Fe to Mg is predicted to build up quickly in the first 1 to 3 Gyr and then level off to the value presently observed in the solar neighbourhood (e.g., Yoshii et al. 1998). More recent studies, however, show that this may be true for our Milky Way and similar galaxies, but can be as short as 0.3 Gyr for elliptical galaxies (Friaca & Terlevich 1998; Matteucci & Recchi 2001), as the time of maximum enrichment is a strong function of the adopted stellar life times, initial mass function, and star formation rate.

Evidence for enrichment on kiloparsec scales is also available from the detection of spatially resolved carbon, oxygen and dust in the interstellar medium around a QSO at $z = 6.4$ (Walter et al. 2003; Bertoldi et al. 2003a; Walter et al. 2004; Maiolino et al. 2005). Simcoe (2006) and Ryan-Weber et al. (2006) have observed two $z \sim 6$ QSOs in the NIR at moderately high spectral resolution and have found several intervening C IV absorption systems, suggesting that Ω_{CIV} does not evolve with redshift. This therefore indicates that even at Mpc scales a large fraction of intergalactic metals may already have been in place at $z > 6$.

As the width of the observed emission lines is believed to represent (at least in part) ordered motion of gas in the very center of the quasars, these can be employed to estimate the mass which drives this motion (see, for example, McLure & Dunlop 2004; Vestergaard & Peterson 2006). The width of the Mg II line is used by several authors to derive masses in the range $1 - 6 \times 10^9 M_{\odot}$ for the central black hole in distant QSOs. For the redshift record holder, quasar SDSS J1148+5251 at $z = 6.42$, this indeed indicates that the quasar is accreting at the maximal allowable rate for a black hole, adopting the Eddington limit criterion (Willott et al. 2003). This quasar has also been detected at mm wavelengths, providing important information about its dust content (Bertoldi et al. 2003a), the mass of the H₂ gas reservoir in the host galaxy (Walter et al. 2003), the density and temperature of CO gas (Bertoldi et al. 2003b) and its dynamical mass (Walter et al. 2004). The estimated dynamical mass of $\sim 5 \times 10^{10} M_{\odot}$ is inconsistent with a $\sim 10^{12} M_{\odot}$ stellar bulge predicted if the $M_{\text{BH}} - \sigma_{\text{bulge}}$ relation (which seems to be valid at lower redshifts, e.g., Gebhardt et al. 2000; Ferrarese & Merritt 2000) were to hold at $z \sim 6$. This indicates that black holes may form prior to the assembly of stellar bulges (Walter et al. 2004). The detection of [C II 158 μm] emission in this QSO by Maiolino et al. (2005) shows that its host is undergoing an intense burst of star formation. Wang et al. (2007) present a sample of eighteen $z \sim 6$ QSOs observed at submm wavelengths. Eight of these are detected at mJy sensitivities, strengthening the idea that massive starbursts exist in quasar host galaxies.

Some of the above mentioned NIR studies have been

hampered by low S/N and/or limited wavelength coverage of the obtained spectra, or included only very few $z \sim 6$ QSOs. With the goal of measuring the physical properties from high-quality observations of a larger number of $z \sim 6$ quasars in a consistent way, we have observed a sample including all published QSOs at redshift $z > 5.8$ and below declination $\delta = +15^\circ$, i.e., those accessible from the four 8m apertures that constitute the Very Large Telescope (VLT). Our NIR ISAAC spectroscopy in several bands from 1.0 to $2.5\mu\text{m}$ covers the C IV, Mg II and Fe II lines. The sample includes objects with lower luminosities than observed in earlier studies and thereby helps to constrain the properties of presumably more *typical* QSOs at these redshifts.

This paper is divided in the following parts: in Sec. 2 we describe the sample, the observations and the data reduction we have carried out. In Sec. 3, the results are shown, including an explanation of the fitting procedure, followed by the measurement of the properties of the spectral features. In Sec. 4, the interpretation of these results is presented, amongst others, in terms of metal enrichment and black hole mass. Finally, we briefly summarize our results in Sec. 5. We assume the following Λ CDM cosmology throughout the paper: $H_0 = 70 \text{ km s}^{-1} \text{ Mpc}^{-1}$, $\Omega_m = 0.3$, $\Omega_b = 0.04$ and $\Omega_\Lambda = 0.7$. These parameters are also used in papers written by McLure & Dunlop (2004) and Vestergaard & Peterson (2006), from which we use several relations.

2. SAMPLE DEFINITION, OBSERVATIONS AND DATA REDUCTION

Of the eleven quasars at $z > 5.8$ known in 2003, we have selected those that are easily observable from the Southern Hemisphere, i.e., at declinations lower than 15° . This resulted in a sample of five targets with magnitudes $18.7 < z_{\text{AB}}^* < 20.5$ and redshifts from discovery papers in the range $5.8 < z < 6.3$ (see Table 1 for names, redshifts, magnitudes and discovery papers).

The observations were carried out with the ISAAC instrument (Moorwood et al. 1998) on Antu (VLT-UT1) in low resolution (LR) mode, using the 1024×1024 Hawaii Rockwell array of the *Short Wavelength* arm. ISAAC's LR grism covers four bands, called *SZ*, *J*, *SH*, and *SK* (referred to as *Z*, *J*, *H* and *K* in this paper). Depending on the order selection filter chosen, this results in spectral resolutions of 550, 500, 500, and 450, respectively, in combination with the $1''$ slit that we have employed (for the *Z*- and *J*-band observations of J1030+0524 and J1306+0356, respectively, we used a narrower $0''.6$ slit resulting in a slightly higher resolution). For each QSO, the C IV and Mg II lines were observed. Depending on the redshift, these lines are in the *Z*- or *J*-band (for J1030+0524), and *K*-band, respectively. For J0836+0054, a spectrum in the *H*-band was also obtained. Table 1 summarizes the bands chosen and the exposure times for each objects. The observations were carried out in service mode and were collected over several years: some of the data were taken as early as May 2001, while the bulk was obtained between October 2004 and March 2006. Exposure times were typically 2.0 hours in *Z*-band and 6.0 hours in *K*-band, but vary from object to object (see Table 1).

In most cases, twenty frames of 120 seconds were exposed in one hour (or observation block), in ABBA se-

quences with large $20''$ to $30''$ offsets (dithering) and small random offsets (jittering to avoid bad pixels, within a box of $4''$ to $18''$). A telluric standard was observed each night (before or after a quasar was observed) at an airmass typically within 0.2 of the airmass of the QSO observations.

The data were reduced using ESO's pipeline software and IRAF. Although ESO delivers the observations together with pipeline reduced products, we have rereduced the original frames using the newest version of ESO's pipeline software (for ISAAC, version 5.4.2) to ensure that all spectra were reduced in the same way. In particular, care was taken that the pipeline reduction was carried out using sky emission lines to determine the wavelength calibration (this was not always the case in the ESO products). Given the short integration times of the telluric stars in the *Z*-band, the imprints of the sky lines were not strong enough to be used as a wavelength indicator, and we thus used the wavelength calibration given by arc lamps observed the following day. The zeropoints of the wavelength scales of the *Z*-band spectra were then corrected by measuring the position of a single bright sky line and, in a few cases, of the hydrogen Paschen lines in the continua of stars serendipitously observed in the same slit as the target.

Rerunning the pipeline produces wavelength calibrated co-added images of the individual frames observed in one observation block. Subsequent reduction was carried out within IRAF. Using IRAF's `apall` task, one-dimensional spectra were extracted from these images. The extraction width was either 5 pixels ($0''.75$) or the seeing FWHM. The spectra were then corrected for telluric extinction using IRAF's `telluric` task (by dividing the observed QSO spectrum by the observed star spectrum), after removal of intrinsic spectral absorption features from the observed star. To get the correct slope and flux calibration, the spectra were multiplied by an artificial black body spectrum of the standard star based on its spectral type and magnitude (in the observed band if available from the literature, but otherwise in the closest band for which a magnitude was available). Then, the individual one-dimensional spectra were averaged to form a single spectrum per quasar per band. The flux calibration of these spectra was checked by comparison with broad band magnitudes. As most of the necessary broad band magnitudes were not available from observations, we fitted the type 1 quasar template SED constructed by Richards et al. (2006b) to the available NIR and MIR photometry from Jiang et al. (2006) and derived *Z*, *J* and *K* flux densities from the resulting normalized SEDs. As the final step in the data reduction, we corrected the absolute flux calibration by factors within the range 0.75 – 2.2 to match these derived broad band fluxes.

3. RESULTS

3.1. Composite spectrum

For illustrative purposes, we have constructed a composite spectrum by shifting the five QSO spectra to their restframe wavelength and averaging them, thereby obtaining a spectrum covering a larger wavelength region than any of the single spectra (Fig. 1). The spectra were normalized to all have the same mean flux density in the

TABLE 1
VLT ISAAC OBSERVATIONS

Full name ^a	Ref ^b	z	$z_{AB}^{*,c}$	$t_{Z}^{\text{exp},d}$ [h]	$t_J^{\text{exp},d}$ [h]	$t_H^{\text{exp},d}$ [h]	$t_K^{\text{exp},d}$ [h]
SDSS J083643.85 + 005453.3	(2)	5.82	18.74	1.7	–	3.2	4.0
SDSS J000552.34 – 000655.8	(3)	5.85	20.54	3.3	–	–	5.3
SDSS J141111.29 + 121737.4	(3)	5.95	19.64	2.0	–	–	6.0
SDSS J130608.26 + 035626.3	(2)	5.99	19.47	1.6	–	–	4.6
SDSS J103027.10 + 052455.0	(2)	6.28	20.05	–	1.6	–	12.0

^a Full names are listed here. In the main text and following tables, only appropriate abbreviations are used, e.g., J0836+0054 for SDSS J083643.85 + 005453.3. ^b Discovery papers, from which redshifts and magnitudes presented in the table have been taken: (1) Fan et al. 2000, (2) Fan et al. 2001, (3) Fan et al. 2004. ^c Magnitudes in z' -band from discovery papers in asinh AB system. Magnitude errors are between 0.05 and 0.10. ^d Exposures time in hours for the bands indicated.

restframe wavelength range 3000 – 3200 Å. As absolute flux reference in this region was taken the spectrum of J0836+0054. Several emission lines are visible, most notable Ly α and Si IV/O IV] in the observed-frame optical domain, and C IV, Mg II and Fe II in the observed-frame NIR domain. To measure the properties of these lines, we must determine the underlying continuum, and, for Mg II, we also need to determine the Balmer pseudo-continuum and the Fe II emission line forest. This spectral decomposition is described in the following section.

3.2. Decomposition of emission lines and continuum

3.2.1. Continuum

The dominant component in the spectra is the continuum, which is usually modelled as a power law ($F_\lambda \propto \lambda^\alpha$). For the quasar composite spectrum obtained from a sample of over 2200 SDSS spectra within a redshift range $0.044 \leq z \leq 4.789$ (see Fig. 2), the slope was found to be $\alpha_\lambda = -1.6$ (Vanden Berk et al. 2001). For individual quasars this value varies, e.g., Richards et al. (2003) find values between -1.75 and -1.24 for most of the 4576 SDSS quasars at $0.3 \leq z \leq 2.2$ in their sample, Pentericci et al. (2003) find a value of -1.43 with a scatter of 0.33 for 45 SDSS quasars at $3.6 \leq z \leq 5.0$, while Maiolino et al. (2004a) find power law slopes between -1.35 and -2.10 for a sample of eight quasars at $4.9 \leq z \leq 6.4$. For spectra with short wavelength coverage and many emission lines (e.g., Mg II, Fe II), the determination of the power law slope is made difficult by the fact that almost no part of the quasar spectrum is not also covered by one or several (blended) emission lines. We, therefore, do fit a power law to be able to measure the flux in the emission lines superposed, but note that the measured slope has a large error and might not be representative for the overall continuum shape of the quasar.

3.2.2. Balmer pseudo-continuum

A second component which has to be determined and subtracted in order to make proper fits to the Mg II and Fe II emission lines, is the forest of hydrogen emission lines, which form the so-called Balmer pseudo-continuum.

To model the Balmer continuum, we have followed Dietrich et al. (2003), who assume gas clouds of uniform temperature ($T_e = 15000$ K) that are partially optically thick. The Balmer continuum spectrum below the

Balmer edge ($\lambda_{BE} = 3646$ Å) can be described by

$$F_\lambda^{\text{BaC}} = F^{\text{BE}} B_\lambda(T_e) (1 - e^{-\tau_{BE}(\lambda/\lambda_{BE})^3}), \lambda \leq \lambda_{BE} \quad (1)$$

where $B_\lambda(T_e)$ is the Planck function at the electron temperature T_e , τ_{BE} is the optical depth at λ_{BE} , and F^{BE} is the normalized flux density at the Balmer edge (Grandi 1982). In general, the normalization is estimated at $\lambda \simeq 3675$ Å since no Fe II emission is present at that wavelength. However, in our spectra, this region is either absent or has a low signal-to-noise ratio. Therefore, the normalization is fixed to the strength of the power-law continuum during the fit and the optical depth is fixed at $\tau_{BE} = 1$ (we found minimal differences in the Balmer continuum when we varied τ_{BE} between 0.1 and 2.0).

3.2.3. Fe II template

The Fe II ion emits a forest of lines, many of which are blended. These are usually fit jointly by using an iron emission line template. Several templates are available in the literature, based on high signal-to-noise ratio spectra of individual active galaxies (e.g., Vestergaard & Wilkes 2001), on composites of many quasar spectra (e.g., from the LBQS by Francis et al. 1991 and from the SDSS by Vanden Berk et al. 2001), or on theoretical models (e.g., Verner et al. 1999; Sigut & Pradhan 2003). Before fitting our data, we have compared two templates applicable to high redshift quasar spectra: one derived from the nearby narrow line Seyfert 1 galaxy, I Zwicky 1, published by Vestergaard & Wilkes (2001) and one we derived from the composite SDSS QSO spectrum (Vanden Berk et al. 2001).

I Zw 1 template by Vestergaard & Wilkes

Vestergaard & Wilkes have constructed an Fe II and Fe III template based on *Hubble Space Telescope* spectra of the narrow line Seyfert 1 galaxy, I Zwicky 1 (I Zw 1, PG 0050+124, $z = 0.061$). Its narrow intrinsic lines (~ 900 km s⁻¹) and its rich iron spectrum make the template particularly suitable for fitting the spectra of active galactic nuclei and quasars. Vestergaard & Wilkes fitted and subtracted a power law continuum, and absorption and emission features from other elements than iron from the I Zw 1 spectrum. An Fe III emission model was subtracted from the residual to create a pure Fe II template. In the process, the Mg II $\lambda\lambda 2795, 2803$ emission was fit with two double Gaussian components 400 km s⁻¹ apart. After subtraction of this Mg II fit, no iron emission is left in the 2770 – 2820 Å range, although

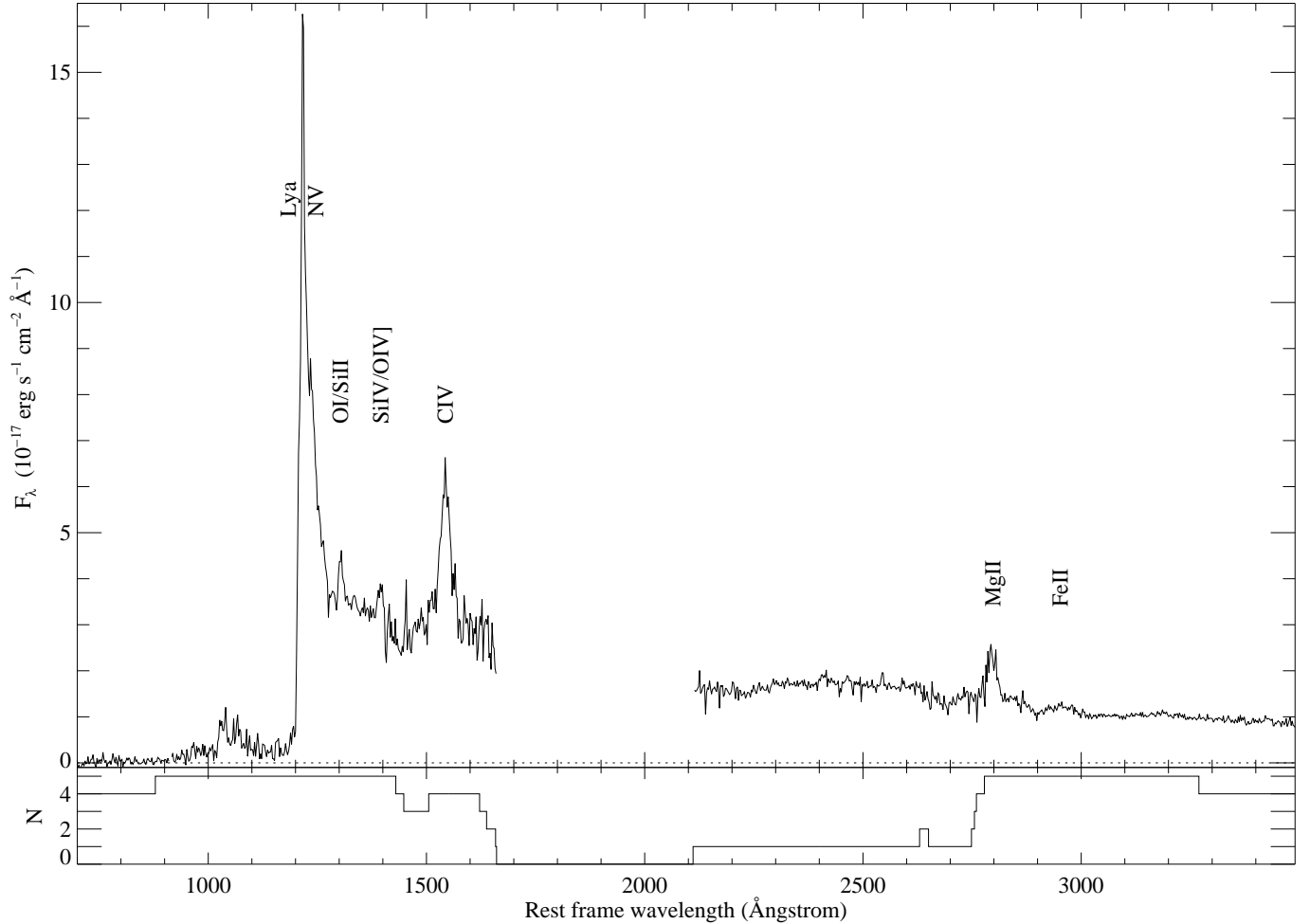


FIG. 1.— Composite spectrum of the five $z \sim 6$ QSOs in our sample at rest frame wavelength. Also displayed is a histogram showing the number of spectra contributing at each wavelength. Strong emission lines are identified. The depression in flux below the Ly α line shows where the GP trough is located (although this is much more pronounced in individual spectra).

from theoretical considerations, it should not be entirely absent. Thus, subtraction of their Fe template would leave some unidentified iron emission around 2800 Å, leading to an overestimate of the flux of the Mg II line. We have therefore added a constant flux density to the Vestergaard & Wilkes template of $\sim 20\%$ of the mean flux density of the template between 2930 and 2970 Å, as illustrated in Fig. 3 (roughly consistent with the value envisaged by Vestergaard & Wilkes 2001). The justification for this operation comes from the theoretical Fe II emission line strength by Sigut & Pradhan (2003, see their Fig. 13).

SDSS QSO composite template by Vanden Berk et al.

From the composite SDSS spectrum, smoothed to a resolution of 7 Å, comparable to the observed rest frame resolution, we have subtracted a power law continuum with the slope given by Vanden Berk et al. (2001). We have normalized the power law to the measured values in the 4200 – 4230 Å region (as specified in Vanden Berk et al. 2001). In addition, a Balmer continuum was created and subtracted, normalized to the measured value at 3675 Å and with optical depth $\tau_{\text{BE}} = 1.0$ (again, only minimal differences were found when changing τ_{BE} within reasonable limits). The result is shown as an inset in Fig. 2.

Comparison of the I Zw 1 and SDSS QSO composite templates

We have subsequently compared the Vestergaard & Wilkes and the SDSS templates (see Fig. 3). The figure shows that the two templates are very similar, apart from the Mg II line which we did not try to subtract in the SDSS template and an Fe III UV47 line at $\lambda = 2418$ Å. We have therefore decided to use the Vestergaard & Wilkes (2001) template for the analysis that follows, as it allows us to fit the Mg II line simultaneously.

3.3. Fitting procedure

Fitting was carried out with the MPFIT³ package which performs the Levenberg–Marquardt least-squares minimization. Nominal errors of the fitted parameters were computed by multiplication of the formal one-sigma errors computed from the covariance matrix with the square root of the reduced χ^2 , which was between 1.0 and 1.5 in all cases.

The K -band spectra were fitted in two steps (see Fig. 4). First, the part of the spectra corresponding to

³ MPFIT is an IDL routine written and distributed by C. Markwardt ([http://cow.physics.wisc.edu/~sim\\$craigm](http://cow.physics.wisc.edu/~sim$craigm)).

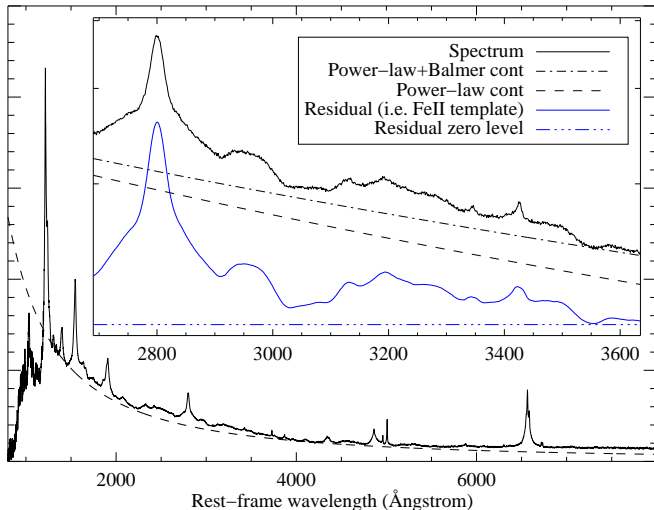


FIG. 2.— The SDSS median quasar composite spectrum (Vanden Berk et al. 2001), shown with an arbitrary flux scaling. The dashed line is a power law continuum ($F_{\lambda} = \lambda^{\alpha}$) with a slope $\alpha = -1.54$ given by Vanden Berk et al. and a normalization fit by us. The inset shows a zoom in the region of the Mg II and part of the Fe II emission. Also shown is the power law continuum and the co-added power law and Balmer continua, which are subtracted from the smoothed composite spectrum to form the final Fe II emission template, shown in grey [blue]. [See the electronic edition of the Journal for a color version of this figure.]

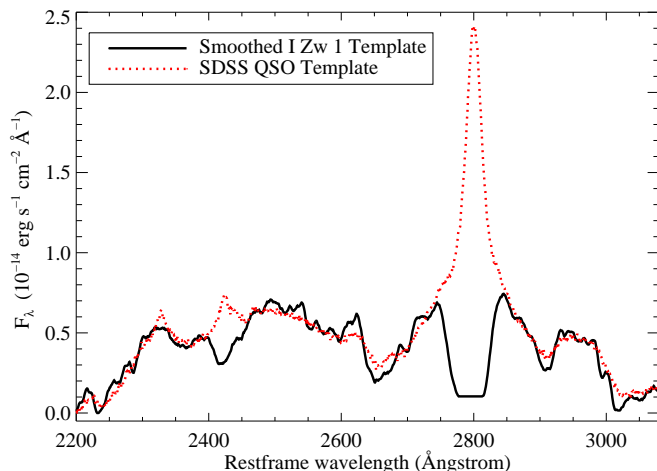


FIG. 3.— Our modified Fe II Vestergaard & Wilkes (2001) template (solid line, smoothed here for display purposes), compared with our template derived from the SDSS composite QSO spectrum (indicated by the dashed [red] line, Vanden Berk et al. 2001). The templates differ significantly only around 2418 Å, where the Fe III UV47 line is located and around 2800 Å, where the prominent Mg II line is located. These lines are not present in the Vestergaard & Wilkes template which contains only Fe II emission. [See the electronic edition of the Journal for a color version of this figure.]

rest-frame wavelengths in the range 2848 to 3081 Å was fit simultaneously by the power-law continuum, Balmer pseudo-continuum and iron template. Here, the Balmer continuum normalization was fixed to the power-law continuum strength at 3600 Å, which leaves only three free parameters being fit at this stage: the slope and normalization of the power-law continuum, and the normalization of the iron template. The iron normalization is mostly determined by the emission feature at ~ 2950 Å. We did not attempt to fit the redshift of the iron template. Instead it was kept fixed (to the Mg II redshift)

and only the template normalization was varied (a few iterations were necessary to obtain this redshift). The fit was then extrapolated to the full spectral range of the K -band spectrum and subtracted from the data. The residual still contains the Mg II line which was subsequently fit with a Gaussian function, having three free parameters: central wavelength, width and normalization. The Fe II flux was computed by multiplying the derived iron template normalization with the total Fe II flux derived from the iron template by integrating it over the wavelength range $2200 < \lambda < 3090$ Å. Here, the assumption is made that the model (the iron template) represents the observed data well. The χ^2 obtained during the fitting procedure gives an indication for this representativeness, but only for the relatively small range $2848 < \lambda < 3081$ Å. Vestergaard & Wilkes (2001) state that the iron template derived from I Zw 1 is generally applicable to high redshift quasar spectra. Our comparison to the SDSS template confirms this. To account for this uncertainty, however, we multiply the nominal error in the Fe II flux by a factor two to obtain the error displayed in Table 2.

The Z and J -band spectra were fitted in one step (see Fig. 5). The C IV line was fit with a Lorentzian function, while the underlying continuum was fit with a power law. The function fit has therefore five free parameters: the power law slope and normalization, and the Lorentzian function's normalization, width and central wavelength. J1411+1217 shows associated absorption in the C IV line, which was fit with a Voigt profile, adding four more free parameters. The fitting parameters are summarized in Table 3.

4. DISCUSSION

4.1. Metal enrichment

As described in Sec. 1, a measurement of the Fe to Mg ratio at $z \sim 6$ may serve as an approximate indication of the onset of star formation in the highest redshift quasars. The measured Fe II/Mg II line ratios of our five $z \sim 6$ QSOs are shown in Table 2. The ratios lie within the range 2 – 5.

We have compared the Fe II/Mg II line ratio measured in our study to those of other studies at similar and lower redshifts (summarized in Fig. 6). It is, however, difficult to make a direct comparison: different studies use different wavelength regions to estimate the underlying continuum and Fe II features and use different methods to fit the spectral features. Iwamuro et al. (2002) try to overcome this problem by applying the same fitting algorithm to new spectra at $4.4 < z < 5.3$ and archival spectra at lower redshifts down to $z = 0.03$. Although the scatter within their redshift bins is large, they measure a median value of Fe II/Mg II at $z \sim 5$ which is about 50% higher than at $z \sim 1.5$. Several other authors have studied the Fe II/Mg II line ratio for QSOs at higher redshifts: $5.7 < z < 6.3$ (Freudling et al. 2003), $3.0 < z < 6.4$ (Maiolino et al. 2003) and $6.1 < z < 6.3$ (Iwamuro et al. 2004). The latter paper summarizes these data and concludes that the upper envelope of the Fe II/Mg II distribution decreases towards higher redshift ($z > 3$) while the scatter among individual objects increases. This may indicate that some objects are observed such a short time after the initial starburst that the Broad Line Region

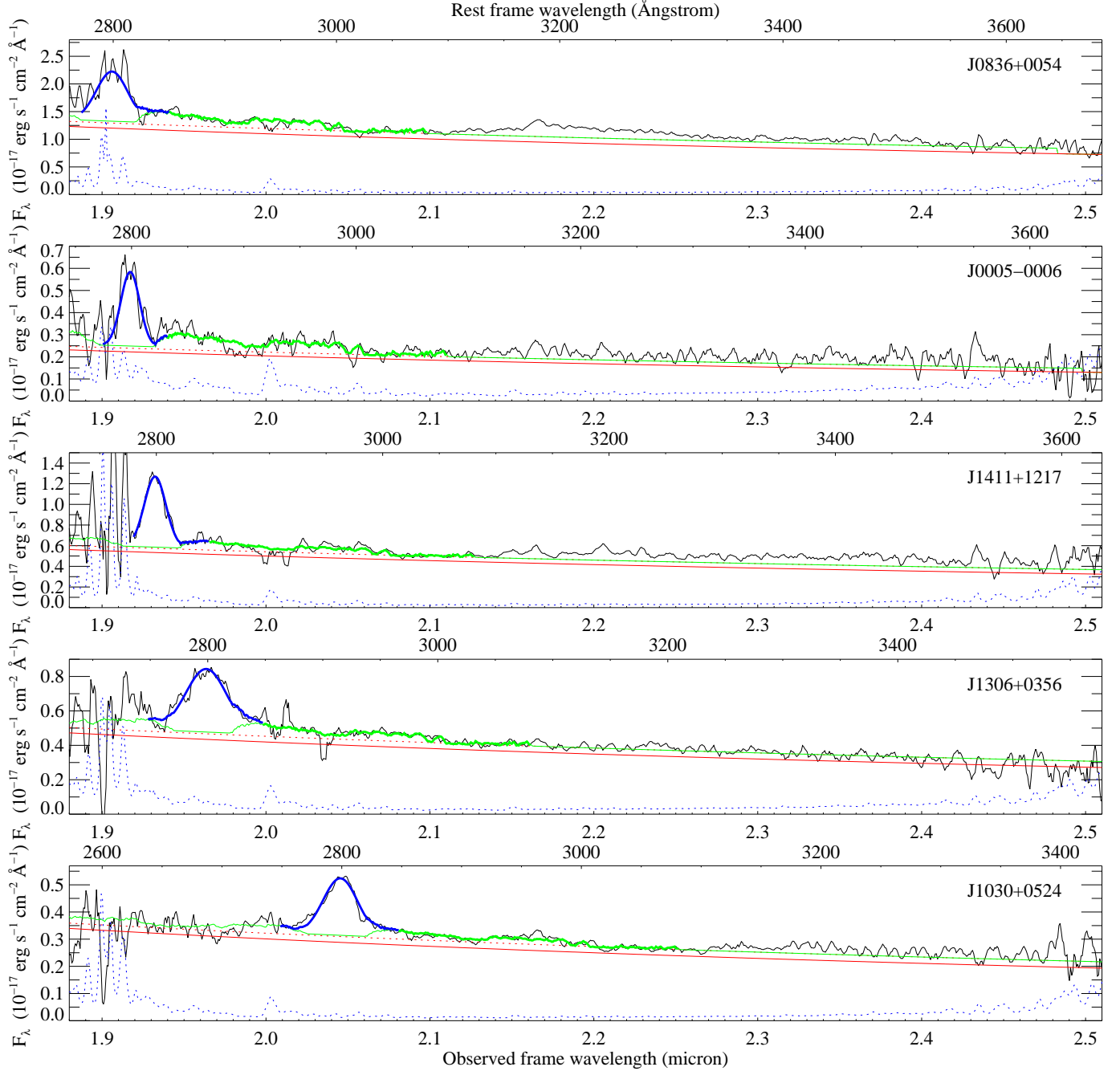


FIG. 4.— K -band spectra of the five $z \sim 6$ QSOs, covering the wavelength region that includes MgII, shown here smoothed over 5 pixels (or $0.0036 \mu\text{m}$). The observed wavelength is indicated below the spectra (in microns), while the rest frame wavelength is indicated above the spectra (in \AA). Several features of the fit are indicated on top of the spectra (dark [black] solid line): the power law continuum (grey [red] solid line), the Balmer pseudo-continuum (grey [red] dashed line), Vestergaard FeII template (light [green] solid line, thick where it is actually fitted to the spectrum), the Gaussian fit to the Mg II line (dark [blue] thick line). The dashed grey [blue] line shows the noise level per pixel (smoothing is not taken into account here). [See the electronic edition of the Journal for a color version of this figure.]

(BLR) is not yet fully enriched with iron. Fig. 6 shows that our measurements confirm the lack of evolution in the Fe II/Mg II line ratio observed by other authors, indicating early enrichment of the BLR. As the age of the Universe at $z = 6.0$ is only 0.9 Gyr, an enrichment time of 1 Gyr needed to reach the observed ratio according to some models (e.g., Yoshii et al. 1998) seems to be ruled out. Assuming an enrichment time of 0.3 Gyr appropriate for an elliptical galaxy (Matteucci & Recchi 2001), the onset of star formation would have been at $z \gtrsim 8$.

Wills et al. (1985) discuss how well the Fe II/Mg II

line ratio represents the Fe/Mg abundance ratio, as the region where Fe II is produced is more extended than the Mg II region, and the radiative transfer of the lines is very different. Computing the Fe II and Mg II line strengths for a range of hydrogen densities and ionization parameters and for a cosmic abundance of elements, they predict values between 1.5 and 4 for the line ratio and attribute higher ratios to an overabundance of iron, with respect to magnesium, but probably also with respect to hydrogen. These computations are, however, based on a limited 70-level model of the iron atom. Baldwin et al.

TABLE 2
FITTED SPECTRAL PROPERTIES OF THE Fe II AND Mg II LINES AND Fe II/Mg II RATIO

QSO	z^a	α^b	F_{FeII}^c 10^{-15} [erg cm $^{-2}$ s $^{-1}$]	z_{MgII}^d	F_{MgII}^e 10^{-15} [erg cm $^{-2}$ s $^{-1}$]	$\text{EW}_{0,\text{MgII}}^f$ [Å]	$\text{FWHM}_{\text{MgII}}$ [km s $^{-1}$]	Fe II/Mg II
J0836+0054	5.82	-1.81	7.4 ± 1.2	5.810 ± 0.003	2.15 ± 0.17	24 ± 3	3600 ± 300	3.4 ± 0.6
J0005-0006	5.85	-2.05	2.3 ± 0.6	5.850 ± 0.003	0.48 ± 0.06	29 ± 5	2100 ± 300	4.7 ± 1.5
J1411+1217	5.95	-1.96	2.7 ± 0.7	5.904 ± 0.002	1.13 ± 0.07	28 ± 3	2400 ± 150	2.4 ± 0.6
J1306+0356	5.99	-1.94	2.4 ± 0.9	6.016 ± 0.002	1.14 ± 0.04	35 ± 2	4500 ± 160	2.1 ± 0.8
J1030+0524	6.28	-1.94	1.2 ± 0.3	6.308 ± 0.001	0.55 ± 0.01	25 ± 1	3600 ± 100	2.1 ± 0.5

^a The redshift as published in the discovery paper, based on the observed wavelength of the Ly α line. ^b Slope of the power law continuum: $F_\lambda \propto \lambda^\alpha$. ^c Flux derived from the Fe II template normalization (derived over the range $2850 \lesssim \lambda_0 \lesssim 3070$ Å). ^d The redshift derived from the Mg II centroid. ^e Flux derived from the Mg II line fit. ^f Rest frame equivalent width of Mg II line in Å.

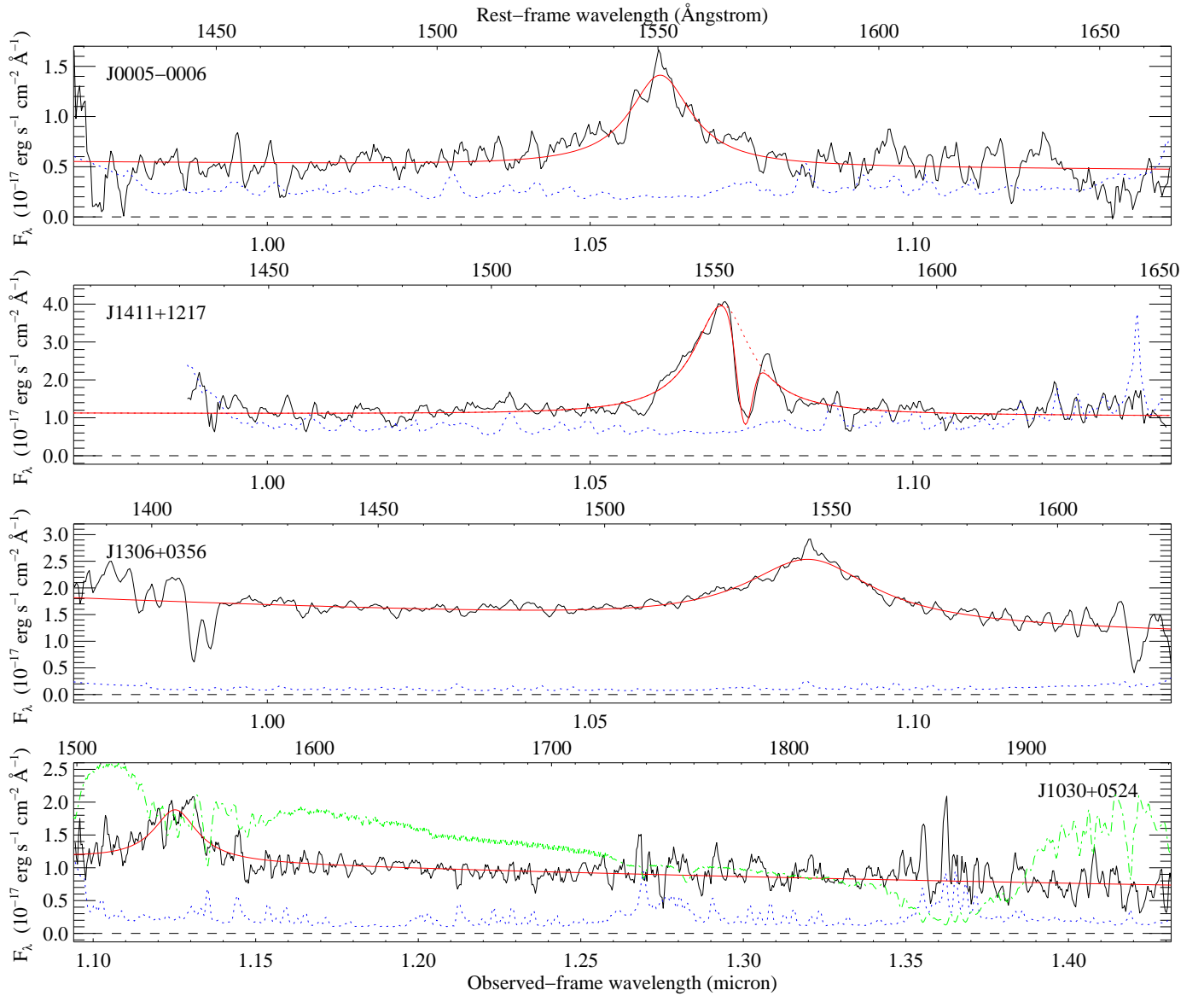


FIG. 5.— Z- and J-band spectra of the five $z \sim 6$ QSOs, covering the wavelength region that includes CIV, smoothed over five pixels (or $0.0014 \mu\text{m}$). Overplotted is the simultaneous fit of a power law and Lorentzian curve (solid [red] line). The absorption feature within the CIV line in J1411+1217 was fitted simultaneously with a Voigt function. The unabsorbed Lorentz profile for J1411+1217 is shown with a dashed line. The dashed [blue] line shows the noise level per pixel (smoothing is not taken into account here). Overplotted on the spectrum of J1030+0524 in grey [green] is the telluric transmission measured, showing the problematic telluric absorption at $1.136 \mu\text{m}$. [See the electronic edition of the Journal for a color version of this figure.]

TABLE 3
FITTED SPECTRAL PROPERTIES OF THE C IV LINE

QSO	z^a	z_{CIV}^b	F^c 10^{-15} [erg cm $^{-2}$ s $^{-1}$]	EW_0^d [Å]	FWHM [km s $^{-1}$]
J0005–0006	5.85	5.848 ± 0.001	1.5 ± 0.1	40 ± 2	2900 ± 140
J1411+1217	5.95	5.911 ± 0.001	5.0 ± 0.1^e	70 ± 3	3060 ± 80
J1306+0356	5.99	5.997 ± 0.001	3.9 ± 0.2	40 ± 2	5940 ± 200
J1030+0524	6.28	6.262 ± 0.003	2.4 ± 0.2	32 ± 3	5030 ± 380

^a The redshift as published in the discovery paper. ^b The redshift derived from the centroid of the C IV line. ^c Flux derived from the C IV line fit. ^d Rest frame equivalent width in Å. ^e Unabsorbed value, actual observed value is smaller.

(2004) construct a 371-level Fe⁺ model, using energy balance to obtain a self-consistent temperature and ionization structure. They apply this model to a large range of parameters in order to reproduce the observed Fe II emission properties and the relative strengths of the strong emission line of other elements (such as Ly α and Mg II). Only two scenarios for observed quasar spectra are allowed by the results of this modeling: there is either significant microturbulence ($v_{\text{turb}} \geq 100$ km s $^{-1}$), consistent with currently popular models where the emission lines are formed in a wind flowing off a rotating accretion disk, or the Fe II lines are formed in gas with other properties than the gas where the other emission lines are formed, i.e., in spatially separated regions. The bottom line is that, although the relative strength of Fe II does depend somewhat (but not linearly, Verner et al. 1999) on the iron abundance, it also depends sensitively on other parameters, preventing strong conclusions on the Fe/Mg abundance ratio from the Fe II/Mg II line ratio, including the comparison with the presumed *solar* value (see Fig. 6).

Although our Fe II/Mg II line ratios are consistent with the values derived by Iwamuro et al. (2004) and Barth et al. (2003), they are systematically lower than those measured by Maiolino et al. (2003). For J1030+0524 our ratio is consistent with that found by Freudling et al. (2003), while for J0836+0054 it is lower. Note that, using the original Fe II template provided by Vestergaard & Wilkes (2001) would result in even lower Fe II/Mg II ratios for our sample (as we would have overestimated the contribution of the Mg II line emission). Within individual studies, the emission line ratios for different $z \sim 6$ quasars also span a large range of values (e.g., 1.0 to 9.5 for Iwamuro et al. and 2.1 to 9.5 for Freudling et al.), indicating that there is significant scatter within the population of $z \sim 6$ quasars. There are several possible causes for the observed discrepancies between different authors, including the iron template employed, the wavelength limits over which the template is integrated, the wavelength range over which the template is actually fit, and the length and signal-to-noise ratio of the spectra used. To derive clear conclusions on the evolution of the Fe II/Mg II line ratio, a better comparison study should be made where all spectra available in the literature are fit by the same template using the same method, but this work is beyond the scope of this paper.

We have found no strong correlations between Fe II/Mg II line ratio, continuum power law slope α

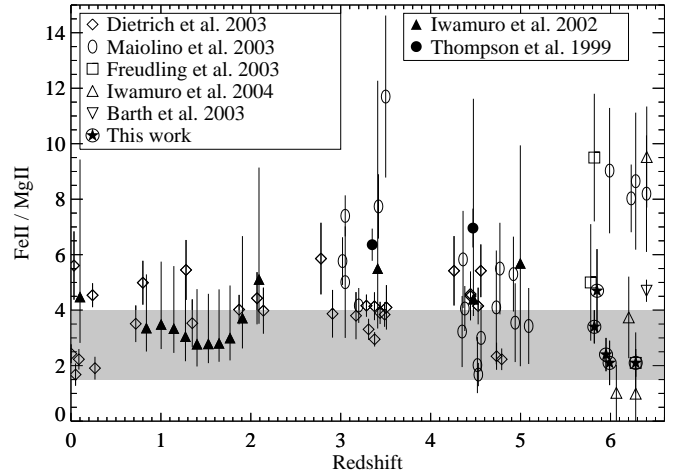


FIG. 6.— Fe II/Mg II line ratio plotted versus redshift of our sample of quasars (encircled stars) compared with quasars at redshifts $0 < z < 6.4$ from the literature: Dietrich et al. (2003, diamonds, including Dietrich et al. 2002), Freudling et al. (2003, squares), Iwamuro et al. (2004, triangles), Thompson et al. (1999, circles), Barth et al. (2003, upside down triangle), Maiolino et al. (2003, ellipses). Filled symbols represent sample averages and their error bars represent the standard deviation of the averages of the measured values. The range of values obtained by modelling the Fe II and Mg II line strengths of gas with cosmic abundance and a range of ionizing continua (2.75 ± 1.25 , see Wills et al. 1985) is indicated by a grey band. See text for details regarding the difference in the determination of this ratio employed by various authors.

and luminosity within our sample. The scatter in the Fe II/Mg II line ratio seems to be small in our sample and independent of luminosity, although the lowest luminosity object is also the iron richest. However, this object, J0005–0006, seems to be peculiar, as it has narrower UV emission lines ($1500 - 2500$ km s $^{-1}$, Fan et al. 2004) than other SDSS QSOs and may not be representative of the general $z \sim 6$ QSO population.

We here summarize the (in)consistencies in measurements by different authors for individual objects in our sample.

Notes on individual objects

J0836+0054 This QSO, at $z = 5.82$ was observed in the NIR by Freudling et al. (2003) and Stern et al. (2003). Freudling et al. (2003) find a (scaled) Fe II/Mg II line ratio of 9.5 ± 2.3 , while the spectrum of Stern et al. (2003) does not include the K -band. We find a ratio of 3.4 ± 0.6 , significantly lower than that found by Freudling et al.

J1306+0356 This QSO, at $z = 5.99$ was observed in the NIR by Maiolino et al. (2003), who found a ratio of 9.0 ± 2.3 , much higher than the value of 2.1 ± 0.8 found by us.

J1030+0524 The most distant QSO of our sample, at $z = 6.28$ was observed in the NIR by Maiolino et al. (2003) and Pentericci et al. (2002). Maiolino et al. (2003), again, find a much higher ratio of 8.7 ± 2.5 than ours of 2.1 ± 0.5 , which, however, is consistent with the value of 2.1 ± 1.1 derived by Freudling et al. (2003) from a NICMOS spectrum sampling rest-frame wavelengths between 1600 and 2700 Å. The ratio derived by us is also consistent with the ratio of $0.99^{+1.86}_{-0.99}$ reported by Iwamuro et al. (2004).

4.2. Black hole masses

The enormous energy output of QSOs is most probably powered by a central black hole which is surrounded by an accretion disc. The mass of this black hole is a fundamental parameter which, at least in nearby galaxies, is strongly correlated with the bulge velocity dispersion of the galaxy host (the so called $M_{\text{BH}} - \sigma_{\text{bulge}}$ relation, where σ_{bulge} is the velocity dispersion of the host galaxy's bulge, e.g., Gebhardt et al. 2000; Ferrarese & Merritt 2000; Tremaine et al. 2002; Woo et al. 2006). This relation suggests that the evolution of the black hole and the build-up of the bulge in its host galaxy are intimately related. The central black hole mass of our Galaxy was measured by very high spatial resolution imaging and subsequent modelling of the stellar dynamics (Schödel et al. 2003), but this method cannot be applied to extragalactic black holes as the required spatial resolution cannot be attained. The most direct measurements of central black holes mass in AGN come from reverberation mapping studies (e.g., Peterson et al. 2004; Kaspi et al. 2007), but these time intensive observations are not easily feasible for very distant QSOs. Here, we derive black hole masses using three different approaches, as described below.

4.2.1. Eddington mass

The simplest method to estimate the black hole mass is to use the bolometric luminosity of the QSO and to assume that the outward radiation pressure gradient acting on the gas is just enough to counterbalance the gravitational attraction of the black hole. This gives an estimate of the black hole mass, called the Eddington mass (Eddington 1922; Margon & Ostriker 1973)

$$L_{\text{Edd}} = 1.3 \times 10^{38} \left(\frac{M_{\text{BH}}}{M_{\odot}} \right) \text{erg s}^{-1}, \quad (2)$$

i.e., the black hole mass M_{BH} can be derived assuming $L_{\text{bol}} = L_{\text{Edd}}$.

4.2.2. Black hole mass derived from Mg II

Under the assumption that the dynamics of the broad line region are dominated by the gravity of the central black hole, an estimate of the black hole mass is given by $M_{\text{BH}} \approx G^{-1} R_{\text{BLR}} V^2$, where M_{BH} is the black hole mass, R_{BLR} the radius of the BLR and V the velocity of the gas, which can be estimated from the width of emission lines in the QSO's spectrum (see McLure & Dunlop 2004 and references therein for a discussion of this assumption and of the emission lines which can be used). The radius of the BLR is strongly correlated with the AGN monochromatic continuum luminosity at 3000 Å (McLure & Jarvis 2002), allowing black hole mass estimates for high redshift quasars to be made from a single spectrum covering the blended Mg II λ 2795,2803 line doublet and redward continuum.

McLure & Dunlop (2004) use 17 AGN (all at $z < 0.7$) with luminosities comparable to those of known high redshift QSOs ($\lambda L_{\lambda} > 10^{37}$ W) for which reverberation mapping estimates of the BH mass are available (from Wandel et al. 1999, and Kaspi et al. 2000), to determine the following relation between black hole mass, continuum luminosity at $\lambda_0 = 3000$ Å and Mg II line width:

$$\frac{M_{\text{BH}}}{M_{\odot}} = 3.2 \left(\frac{\lambda L_{3000}}{10^{37} \text{ W}} \right)^{0.62} \left(\frac{\text{FWHM} [\text{MgII}]}{\text{km s}^{-1}} \right)^2, \quad (3)$$

where L_{3000} is the luminosity per wavelength bin at rest-frame $\lambda_0 = 3000$ Å and FWHM is the Full Width at Half Maximum of the Mg II line. McLure & Jarvis (2002) state that an earlier version of this black hole mass estimator can reproduce the reverberation black hole mass to within a factor 2.5 (1σ).

4.2.3. Black hole mass derived from C IV

Vestergaard & Peterson (2006) use 32 AGN with reliable reverberation mapping estimates calculated by Peterson et al. (2004) to derive the following empirical relation between black hole mass, continuum luminosity at $\lambda_0 = 1350$ Å, and C IV line width:

$$\frac{M_{\text{BH}}}{M_{\odot}} = 4.6 \left(\frac{\lambda L_{1350}}{10^{37} \text{ W}} \right)^{0.53} \left(\frac{\text{FWHM} [\text{CIV}]}{\text{km s}^{-1}} \right)^2. \quad (4)$$

Vestergaard & Peterson estimate that this mass estimator is accurate within a factor 3.6 – 4.6, but they also note that the reverberation-based masses themselves are uncertain typically by a factor ~ 2.9 .

It should be noted that some authors (e.g., Baskin & Laor 2005) have argued that the C IV originates, at least in part, from outflowing gas or that the shift and asymmetry commonly seen in C IV suggest that non-gravitational effects, such as obscuration and radiation pressure, may affect the line profile (e.g., Richards et al. 2002b) and its FWHM would therefore not be a good measure of the gas dynamics in the BLR, although Vestergaard & Peterson (2006) claim that the typical uncertainties resulting from these are smaller than those quoted above for the mass estimator itself.

4.2.4. Derived black hole masses

Using these three approaches, we estimate black hole masses for our sample and list them in Table 4. The bolometric luminosities for these quasars were obtained by Jiang et al. (2006) from SED template fits to combined observations at wavelengths including the radio, mm/submm, UV/optical, NIR, MIR and X-rays. For the computation of L_{1350} , we had to extrapolate the continuum measured to the wavelength required using the fitted power law, but given the fact that the continuum is well characterized in the Z- and J-band, this should not introduce large errors. The black hole masses for the sample at hand range from 0.3 to $5.2 \times 10^9 M_{\odot}$, including the lowest black hole masses ever observed for $z \sim 6$ QSOs. In general, the black hole masses derived using the three different techniques agree within a factor of a few, where the mass derived from the C IV line is largest and the Eddington mass in between. We note that, even in the absence of any measurement errors, the individual BH mass estimates have an uncertainty of a factor ~ 3 from the scatter in the correlations measured by McLure & Dunlop (2004) and Vestergaard & Peterson (2006).

If the quasars were strongly lensed, the mass derived by the Eddington luminosity would be larger by \sqrt{q} , where q is the lensing factor, as $M_{\text{Edd}} \sim q$ and $M_{\text{MgII/CIV}}$ roughly scales with \sqrt{q} . Assuming that quasars emit isotropically (which may not be the case, see Hennawi & Prochaska 2007), the good agreement between the different black hole mass estimates implies that the quasars are likely not strongly lensed, consistent with

TABLE 4
ESTIMATED BLACK HOLE MASSES

QSO	z^a	$M_{\text{BH}}(\text{Mg II})$ [$10^9 M_\odot$]	$M_{\text{BH}}(\text{C IV})$ [$10^9 M_\odot$]	$M_{\text{BH}}(\text{Edd})$ [$10^9 M_\odot$]
J0836+0054	5.82	2.7 ± 0.6		4.0
J0005-0006	5.85	0.3 ± 0.1	0.7 ± 0.1	0.7
J1411+1217	5.95	1.1 ± 0.1	1.2 ± 0.2	1.2
J1306+0356	5.99	2.4 ± 0.4	5.2 ± 0.7	1.9
J1030+0524	6.28	1.4 ± 0.2	3.2 ± 0.6	1.8

^a The redshift as published in the discovery paper.

the conclusions derived from an analysis of HST images of these objects, none of the QSOs showing evidence for lensed counterparts (Richards et al. 2004, 2006a). For J1030+0524, Haiman & Cen (2002) predict a minimum BH mass of $\sim 10^9 M_\odot$ based on the flux distribution of the Ly α emission alone and assuming it is not gravitationally lensed. The BH mass derived by us for this quasar is in the range $1.4 - 3.2 \times 10^9 M_\odot$, consistent with the prediction by Haiman & Cen (2002).

Black hole masses derived from the observed-frame NIR emission lines for the QSOs in our sample have not been reported in the literature, although for some of the sources the C IV line has been observed (J0836+0054 by Stern et al. 2003, J1306+0356 by Maiolino et al. 2004a and Pentericci et al. 2002, J1030+0524 by Maiolino et al. 2004a). We can compare, however, with the BH mass measured for the $z = 6.4$ QSO J1148+5251, which was measured by Barth et al. (2003) and Willott et al. (2003), employing relations between the Mg II and C IV line widths and black hole masses very similar to those employed by us. These authors find a BH mass of $(2 - 6) \times 10^9 M_\odot$ and $3 \times 10^9 M_\odot$, respectively. The BH masses measured by us are in general smaller, showing that we sample the BH mass function to lower masses than previous studies, probing not only the most massive and luminous objects but also the presumably more common less massive quasars.

4.3. Redshifts of QSOs in our sample

For several reasons, it is useful to know the systemic redshift of a QSO with high precision, e.g., for follow-up observations of molecular lines with narrow bandpasses. The systemic redshift is difficult to derive from the centroid of the observed Ly α line, as it is very susceptible to absorption by neutral hydrogen on its blue side, can be blended with the N V line or because it is completely absent. Narrow emission lines due to star formation are more suitable redshift indicators. For example, the [O III] $\lambda 5007$ line is presumed to be at nearly the systematic redshift of the host galaxy (see Sec. 3.0 of Vanden Berk et al. 2001, for references). If narrow lines cannot be observed, broad QSO emission lines other than Ly α can give important information about the systemic redshift of the galaxy observed. Using the redshift of [O III] $\lambda 5007$ as a zeropoint, Vanden Berk et al. (2001) find an average redshift offset of 143 ± 91 and 161 ± 10 km s $^{-1}$ for Ly α and Mg II and a blueshift offset of 563 ± 27 km s $^{-1}$ for C IV (where the errors indicate uncertainties in the mean value, the intrinsic scatter is much larger).

Richards et al. (2002b) study these offsets in more detail and find a redshift offset of 97 km s $^{-1}$ for Mg II and a blueshift offset of 727 km s $^{-1}$ for C IV, with dispersions

TABLE 5
REDSHIFT MEASUREMENTS

QSO	z^a	$z_{\text{C IV}}$	$z_{\text{Mg II}}$	z_{sys}^b
J0836+0054	5.82	—	5.810 ± 0.003	5.808 ± 0.007
J0005-0006	5.85	5.848 ± 0.001	5.850 ± 0.003	5.848 ± 0.007
J1411+1217	5.95	5.911 ± 0.001	5.904 ± 0.002	5.902 ± 0.007
J1306+0356	5.99	5.997 ± 0.001	6.016 ± 0.002	6.014 ± 0.007
J1030+0524	6.28	6.262 ± 0.003	6.308 ± 0.001	6.306 ± 0.006
δv^c (km s $^{-1}$)		-193	97	
δz^d		0.005	-0.002	

^a The redshift as published in the discovery paper. ^b Systemic redshift estimate based on corrected Mg II redshift. ^c Velocity difference between the listed line and the [O III] $\lambda 5007$ centroid (from Vanden Berk et al. 2001 for Ly α and N V, from Richards et al. 2002b for C IV and Mg II). ^d Correction in redshift for $z = 6.0$.

of ± 269 and ± 511 km s $^{-1}$, respectively. Their analysis shows that the apparent shift of the C IV line peak is not so much a shift as it is a lack of flux in the red wing. They also confirm the observed anticorrelation between the shift of the C IV line peak and the rest equivalent width of this line. Richards et al. present this correlation as follows: they first sorted their list of 794 quasars according to their C IV–Mg II redshift differences and then divided this list into four roughly equal bins with ~ 200 quasars each. The four bins, having C IV EW $_0$ s of 30.3, 25.8, 22.3, 18.0 Å, have average blue shifts of 193, 651, 1039, 1596 km s $^{-1}$ with respect to the Mg II line peak, respectively. As all our measured C IV EW $_0$ s are larger than 30 Å, we assume the C IV line is blue shifted by 96 km s $^{-1}$ with respect to the systemic velocity. As the shifts of line peaks of emission lines in the spectrum of an individual quasar are correlated, one can obtain a better redshift correction if the peak wavelengths of several lines are measured (see Shen et al. 2007), but we do not apply this method as we do not have enough suitable lines with a high enough signal-to-noise ratio in our spectra.

Table 5 presents for each QSO, the observed C IV and Mg II redshift and the systemic redshift z_{sys} , which is equal to the Mg II redshift corrected as described above (i.e., $+97$ km s $^{-1}$). The error on the systemic redshift takes into account the dispersion found by Richards et al. (2002b) for the offset of Mg II (i.e., ± 269 km s $^{-1}$). Relatively large inconsistencies remain between the corrected redshifts of C IV and Mg II. One cause could be that C IV, being a resonant line, can potentially suffer from absorption, as is the case for J1411+1217 (see Fig. 5).

Notes on individual objects

J0836+0054 This QSO was observed by Stern et al. (2003). From the C III $\lambda 1909$ line, Stern et al. (2003) derive a corrected⁴ redshift of $z = 5.774 \pm 0.003$. This is quite different from our systemic redshift of $z_{\text{sys}} = 5.808 \pm 0.007$. Freudling et al. (2003) measure an uncorrected C III $\lambda 1909$ and Mg II redshift of $z = 5.82$ from their low resolution NICMOS spectrum.

J1306+0356 Measurements to the same data presented here were published by Pentericci et al. (2002), who find an uncorrected C IV redshift of $z = 6.00 \pm 0.01$, consistent with our result and with the value derived from N V by

⁴ Using the 224 km s $^{-1}$ velocity difference with [O III] $\lambda 5007$ found by Vanden Berk et al. (2001)

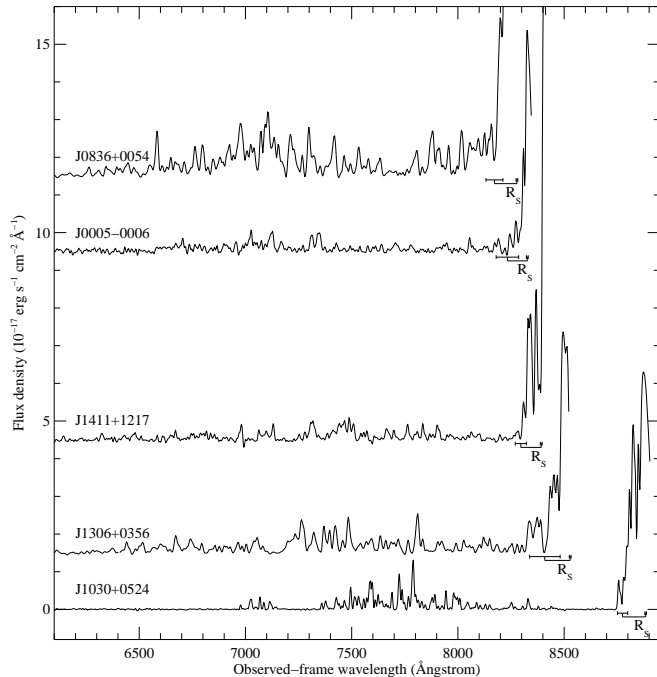


FIG. 7.— Optical spectra of the quasars in our sample, offset in the vertical direction for clarity by 1.5, 4.5, 9.5, and 11.5 $\times 10^{-17}$ $\text{erg s}^{-1} \text{cm}^{-2} \text{\AA}^{-1}$. The size of the Strömgren sphere (R_s) is indicated by the line which connects the measurements of the onset of the Gunn–Peterson (GP) trough (z_{GP}) and the systemic redshift (z_{sys}) derived from the Mg II line. Error bars for both the GP trough onset and the systemic redshift have been indicated, although the uncertainties on the latter are too small for the error bars to be discernable for most quasars.

Becker et al. (2001).

J1030+0524 Freudling et al. (2003) measure an uncorrected C III] $\lambda 1909$ and Mg II $\lambda 2800$ redshift of $z = 6.28$ from their low resolution NICMOS spectrum. Iwamuro et al. (2004) find an uncorrected Mg II redshift of $z = 6.311$ (and do not report the uncertainty). Pentericci et al. (2002) derive uncorrected redshifts of $z = 6.29 \pm 0.01$ and 6.27 ± 0.02 from N V and C IV, respectively, while we find a consistent redshift of $z = 6.262 \pm 0.003$ (uncorrected) from C IV.

4.4. The size of the ionized sphere around the QSO

At $z \sim 6$, most of a quasar’s emission below the Ly α line is absorbed by neutral hydrogen in the IGM. However, the quasar is able to ionize a (Strömgren) sphere around it, from which it transmits radiation at wavelengths below that of the Ly α line. The red edge of the GP trough marks the radius of this sphere. Therefore, the radius of the Strömgren sphere can be derived from the difference between the redshift of this red edge and the systemic redshift. However, if the GP effect is not complete, the precise redshift z_{GP} of the red edge may be difficult to determine and may depend on the spectral resolution of the observations. We have tried to determine z_{GP} conservatively by eye, determining where the Ly α emission from the QSO may be fully absorbed, but including in its error the range of redshifts where this plausibly could happen. This results in relatively large error bars for some QSOs in our sample, as shown in Fig. 7. As the uncertainty in z_{GP} is much larger than the uncertainty in the systemic redshift, we disregard the latter in the following computation.

The Strömgren sphere radius (R_s) is equal to the physical distance between z_{sys} and z_{GP} (see Hogg 1999):

$$R_s = \frac{D_H}{(1+z)} \int_{z_{\text{GP}}}^{z_{\text{sys}}} (\Omega_m(1+z)^3 + \Omega_\Lambda)^{-1/2} dz, \quad (5)$$

where D_H is the Hubble distance and Ω_m and Ω_Λ the ratios of the mass and vacuum energy density to the critical density, respectively. For the cosmological parameters used here and a redshift $z = 6.0$, we obtain $R_s = 60 (z_{\text{sys}} - z_{\text{GP}})$ Mpc. The derived values of R_s for our sample are listed in Table 6.

4.5. QSO activity time scales

The size of H II regions around a luminous quasar, prior to complete reionization, depends on the ionizing photon emission rate (\dot{N}_{ph}), the time span the ionization is sustained (t_Q) and the density of neutral hydrogen ($n_{\text{H}} x_{\text{HI}}$) in which the sphere expands

$$R_s \approx \left(\frac{3 \dot{N}_{\text{ph}} t_Q}{4\pi n_{\text{H}} x_{\text{HI}}} \right)^{1/3} \quad (6)$$

where x_{HI} is the neutral hydrogen fraction. This formula results from matching the total number of ionizing photons emitted to the number of hydrogen atoms within a sphere, and it ignores both recombinations and the Hubble expansion (White et al. 2003, see Maselli et al. 2007 for a discussion of the validity of the assumptions made here). If the quasar is located in a region overdense by a factor D , the radius is reduced by $D^{-1/3}$ (White et al. 2003). Furthermore, from the analysis of mock spectra along lines of sight through a simulated QSO environment, Maselli et al. (2007) find that the H II region size derived from quasar spectra is on average 30% smaller than the physical one. Note that issues of geometry, H I clumping factor, and pre-QSO reionization by, e.g., star forming galaxies in the QSO vicinity, further complicate a conversion from observed Strömgren sphere radius to quasar activity time. As we are interested only in order of magnitude effects, we do not take these issues into account.

Assuming that the quasar is located in a completely neutral IGM (i.e., $x_{\text{HI}} \sim 1$) which contains nearly all the baryons (i.e., n_{H} is equal to the mean cosmic density at $z = 6$), Cen & Haiman (2000) and Haiman & Cen (2002) use the the radius of the Strömgren sphere to constrain the minimum activity time for the quasar

$$t_Q = \left(\frac{\dot{N}_{\text{ph}}}{10^{57} \text{ s}^{-1}} \right)^{-1} \left(\frac{R_s}{7.4 \text{ Mpc}} \right)^3 \left(\frac{1+z}{7.0} \right)^3 10^8 \text{ yr.} \quad (7)$$

Note that this time is very short, and of the order of the light crossing time of the Strömgren sphere. White et al. (2003) explain that the speed of light drops out of the equations describing the early evolution of a Strömgren sphere, and that, for an observer, there is an initial period of superluminal expansion.

The ionization rate depends on the SED below (blueward of) the Ly α line, which we estimated from the SED above 1216 \AA . The composite quasar SED of Elvis et al. (1994) with median bolometric luminosity $10^{44} \text{ erg s}^{-1}$ has a corresponding median $\dot{N}_{\text{ph}} = 5.5 \times 10^{53}$ photons

TABLE 6
STRÖMGREN SPHERE RADII AND QUASAR ACTIVITY TIME SCALES

QSO	z^a	M_{1450}^b	z_{GP}	z_{sys}	R_S [Mpc]	$\dot{N}_{ph,Elv}$ [10^{57} s^{-1}]	$t_{Q,Elv}$ [10^7 yr]	$t_{Q,Tel}$ [10^7 yr]
J0836+0054	5.82	-27.83	5.721 ± 0.033	5.808	5.7 ± 2.2	4.70	0.6	0.1
J0005-0006	5.85	-26.42	5.771 ± 0.044	5.848	4.9 ± 2.8	0.47	3.9	0.8
J1411+1217	5.95	-26.70	5.823 ± 0.021	5.902	5.0 ± 1.4	1.07	1.8	0.4
J1306+0356	5.99	-27.14	5.916 ± 0.059	6.014	5.9 ± 3.6	1.40	2.4	0.5
J1030+0524	6.28	-27.10	6.217 ± 0.020	6.306	4.9 ± 1.1	1.35	1.4	0.3

^a The redshift as published in the discovery paper. ^b AB magnitude at rest-frame wavelength 1450 Å from the discovery papers, corrected for the cosmology used here. ^c Redshift from the centroids of the CO lines measured by Walter et al. 2003 and Bertoldi et al. 2003b.

s^{-1} . We have used this relation to derive the ionization rates for our sample QSOs ($\dot{N}_{ph,Elv}$, see Tab. 6). From these ionization rates and Eq. 7 we derive minimum activity times for the quasars in the range: $t_{Q,Elv} \sim 0.6 - 9 \times 10^7 \text{ yr}$. However, as noted by White et al. (2003), who have used the quasar templates by Telfer et al. (2002), the ionization rates by Elvis et al. may be too low by a factor of five. Consequently, the quasar activity times derived from the Strömgren spheres would go down by the same factor: $t_{Q,Tel} \sim 0.1 - 2 \times 10^7 \text{ yr}$ (see last column of Tab. 6). For a partly ($x_{HI} = 0.1$, Wyithe et al. 2005) or even mostly ($x_{HI} = 0.01$, Maselli et al. 2007) ionized IGM at $z \sim 6$, the derived activity times are smaller by a factor 10 or even 100.

We can now compare these ages to the e-folding time scale for the central accreting black hole (the *Salpeter time scale*, Salpeter 1964)

$$t_{acc} = 4 \times 10^7 \left(\frac{\epsilon}{0.1} \right) \eta^{-1} \text{ yr} \quad (8)$$

where ϵ is the radiative efficiency and η is the ratio of quasar to Eddington luminosity (Haiman & Loeb 2001, see also the discussion in White et al. 2003). Assuming that the quasar is radiating at the Eddington limit ($\eta \sim 1$) and an efficiency of $\epsilon \sim 0.1$, this simple calculation gives values that are consistent, to first order, with our derived ages of the Strömgren spheres in a neutral IGM. This implies that the mass of the central black hole in the quasars observed grows only by one e-folding or less during one quasar activity cycle.

4.6. Absorption features

No Broad Absorption Lines (BALs) are found in the spectra, although the C IV emission line of J1411+1217 shows associated C IV absorption. The blue shifted BALs in QSOs are probably caused by an outflowing wind. At low and intermediate redshift, BAL QSOs account for $\sim 15\%$ of the whole quasar population (Reichard et al. 2003; Hewett & Foltz 2003), but Maiolino et al. (2004a) find four BAL QSOs among the eight QSOs at $4.9 < z < 6.4$ that they observe, suggesting that the most distant quasars are surrounded by a much larger amount of dense gas than lower redshift quasars. Adding the three QSOs without C IV BALs of our sample (J1030+0524 was already found to be non-BAL by Maiolino et al.), the fraction of BAL QSOs at $z > 4.9$ (5.7) goes down to 36% (25%). A larger sample of $z \sim 6$ QSOs with C IV spectroscopy is needed to resolve this issue.

While not immediately the science focus of this paper, we have also searched for narrow absorption lines of

intervening systems. The spectral resolution of $\sim 20 \text{ Å}$ in our spectra does not allow to identify the C IV doublet (see Simcoe 2006; Ryan-Weber et al. 2006), but it is good enough to resolve the redshifted lines of the Mg II $\lambda 2796, 2803$ system. Within the continuum emission of the QSO J1306+0356, we find two systems of double absorption lines: at 9797.7, 9827.4 Å and 9880.7, 9906.3 Å with observed EWs of 6.2, 4.0, and 11.6, 10.3 Å, respectively. In addition, a third system of double absorption may be present at the red edge of the *J*-band spectrum: at 11340.6, 11401.2 Å with observed EWs of 13, 11 Å, respectively (see Fig. 8). These absorption features would be consistent with Mg II absorption at $z = 2.504, 2.533$ and 3.060 (although the latter only marginally), but a systematic search with larger wavelength coverage by Jiang et al. (2007, AJ, in press) shows that the correct identifications for the first double absorption feature is Al II 1670 at $z = 4.864$ and 4.882, while the third double absorption feature may be Fe III 1926 from the same intervening systems. We note, however, that the latter lines are at the edge of the observed spectrum where the noise is higher and the wavelength calibration is not very accurate. The second double absorption feature is indeed confirmed to be Mg II at $z = 2.533$ from other absorption lines identified. The two absorbers at $z = 4.9$ are the highest redshift Mg II absorbers known (see, e.g., Kobayashi et al. 2005). See Jiang et al. for more details and a discussion on the absorber host galaxies.

4.7. Continuum slope

The continuum slopes are measured over small wavelength intervals with little pure continuum emission, especially for the *K*-band spectra. Despite resulting uncertainties, the measured slopes lie in the range $-2.06 < \alpha < -1.83$, steeper than that measured by Vanden Berk et al. (2001, -1.54) for the SDSS composite QSO spectrum at a median $z = 1.3$ and than that measured from NIR photometry of 45 QSOs at $3.6 < z < 5.3$ by Pentericci et al. (2003, -1.43 ± 0.33). Maiolino et al. (2004a) find such steep continuum slopes for some of their QSOs at $4.95 < z < 6.40$, and in particular for J1048+4637 at $z = 6.19$, where they measure a slope of $\alpha = -2.1$ at rest frame wavelength above 1700 Å (Maiolino et al. 2004b). Jiang et al. (2007, AJ, in press) observe a $z \sim 6$ QSO sample with larger wavelength coverage and are therefore able to constrain the continuum slopes better, obtaining results similar to ours.

5. SUMMARY AND CONCLUSIONS

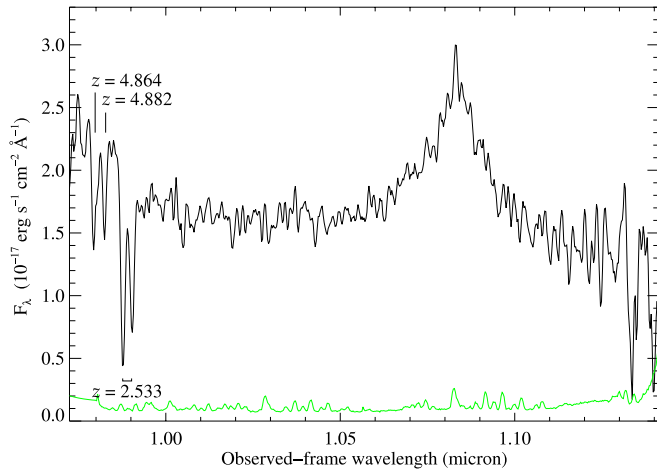


FIG. 8.— Z-band spectrum of J1306+0356, smoothed over three pixels, with AlII absorption from systems at $z = 4.864$ and 4.882 and MgII absorption at $z = 2.533$ indicated. The grey [green] line shows the noise per pixel. [See the electronic edition of the Journal for a color version of this figure.]

We present sensitive near-infrared spectroscopic observations of a sample of five $z \sim 6$ quasars, comprising all published quasars at $z > 5.8$ accessible from the VLT. Our ISAAC spectra cover the C IV, Mg II and Fe II lines, which are powerful probes of the chemical enrichment and the black hole masses in these objects. As the Mg II and Fe II lines are blended (and are located on top of the Balmer continuum), we have used Fe templates derived from an SDSS composite quasar spectrum (Vanden Berk et al. 2001) and from the spectrum of I Zw 1 (Vestergaard & Wilkes 2001) and simple models representing the continuum and Balmer pseudo-continuum to decompose the spectra. We derive an average Fe II/Mg II (which is a proxy for the Fe/ α) ratio of 2.7 ± 0.8 for our sample, which is similar to the values measured for quasar broad line regions at lower redshifts. We note that the values measured by us are lower by a factor of a few than some previous measurements for individual quasars at $z > 5.8$ reported in the literature (Maiolino et al. 2003; Freudling et al. 2003; Iwamuro et al. 2004) but are consistent with others (Barth et al. 2003; Freudling et al. 2003; Iwamuro et al. 2004). We attribute these differences to different choices in the Fe templates used, the corresponding spectral decomposition and the different quality of the spectra. The lack of evolution in the observed Fe II/Mg II ratio and the mere presence of iron in the $z \sim 6$ systems demonstrate that the quasars in our sample must have undergone a major episode of iron enrichment in the short time span between the Big Bang and the emission of radiation observed by us, i.e., in less than one Gyr, consistent

with the conclusions derived by previous studies (see also Barth et al. 2003; Maiolino et al. 2003; Freudling et al. 2003).

We have derived central black hole masses using three different methods: A) using the Eddington luminosity, B) using the empirical equation relating the linewidth of Mg II (and the nearby continuum emission) to the mass of the black hole (McLure & Dunlop 2004) and C) using the corresponding method for the CIV line (Vestergaard & Peterson 2006). The derived masses using the Mg II and C IV lines and the Eddington luminosity agree well, and we derive central black hole masses of $0.3 - 5.2 \times 10^9 M_\odot$. Our derived black hole mass range includes the lowest black hole mass ever measured at $z \sim 6$ and indicates that we have started to probe the more typical quasar population (with lower masses/luminosities) at this extreme redshift. Clearly, future, more sensitive, observations of an extended sample towards lower luminosities are needed to constrain the properties of the fainter quasar population further. Assuming that the quasars indeed radiate at their Eddington luminosity, the agreement in derived black hole masses using the different methods implies that the quasars are likely not strongly lensed and emit roughly isotropically.

We use the difference between the redshift derived from the Mg II line, which serves as the best available proxy for the systemic redshift of the quasar, and the redshift for the onset of the GP trough in the quasar spectra to derive the extent of the ionized Strömgren spheres around our target quasars. The derived physical radii are relatively well constrained to about five Mpc. Using simple ionization models, the central quasar activity would need of order $10^6 - 10^8$ yr to create these cavities, allowing the quasar black hole to grow by one e-folding or less during an activity cycle.

JK is supported by the DFG, Sonderforschungsbereich (SFB) 439. DR acknowledges support from DFG Priority Programme 1177. MAS acknowledges support from NSF grant AST-0307409. We are grateful to Marianne Vestergaard for providing the electronic version of her Fe II template (Vestergaard & Wilkes 2001). Based on observations carried out at the European Southern Observatory, Paranal, Chile under program Nos. 267.A-5689, 069.B-0289, 071.B-0525, 074.A-0477 and 076.A-0304.

Facilities: VLT (ISAAC).

REFERENCES

- Aoki, K., Murayama, T., & Denda, K. 2002, PASJ, 54, 353
 Baldwin, J. A., Ferland, G. J., Korista, K. T., Hamann, F., & LaCluyzé, A. 2004, ApJ, 615, 610
 Barth, A. J., Martini, P., Nelson, C. H., & Ho, L. C. 2003, ApJ, 594, L95
 Baskin, A. & Laor, A. 2005, MNRAS, 356, 1029
 Becker, R. H., Fan, X., White, R. L., Strauss, M. A., Narayanan, V. K., Lupton, R. H., Gunn, J. E., Annis, J., et al. 2001, AJ, 122, 2850
 Bennett, C. L., et al. 2003, ApJ, 583, 1
 Bertoldi, F., Carilli, C. L., Cox, P., Fan, X., Strauss, M. A., Beelen, A., Omont, A., & Zylka, R. 2003a, A&A, 406, L55
 Bertoldi, F., et al. 2003b, A&A, 409, L47
 Cen, R. & Haiman, Z. 2000, ApJ, 542, L75
 Dietrich, M., Appenzeller, I., Vestergaard, M., & Wagner, S. J. 2002, ApJ, 564, 581
 Dietrich, M., Hamann, F., Appenzeller, I., & Vestergaard, M. 2003, ApJ, 596, 817
 Eddington, A. S. 1922, MNRAS, 83, 32
 Elvis, M., et al. 1994, ApJS, 95, 1
 Fan, X. 2006, New Astronomy Review, 50, 665
 Fan, X., Carilli, C. L., & Keating, B. 2006a, ARA&A, 44, 415
 Fan, X., et al. 2004, AJ, 128, 515
 Fan, X., et al. 2001, AJ, 122, 2833
 Fan, X., et al. 2006b, AJ, 132, 117
 Fan, X., et al. 2006c, AJ, 131, 1203

- Fan, X., et al. 2003, *AJ*, 125, 1649
 Fan, X., et al. 2000, *AJ*, 120, 1167
 Ferrarese, L. & Merritt, D. 2000, *ApJ*, 539, L9
 Francis, P. J., Hewett, P. C., Foltz, C. B., Chaffee, F. H., Weymann, R. J., & Morris, S. L. 1991, *ApJ*, 373, 465
 Freudling, W., Corbin, M. R., & Korista, K. T. 2003, *ApJ*, 587, L67
 Friaca, A. C. S. & Terlevich, R. J. 1998, *MNRAS*, 298, 399
 Gebhardt, K., et al. 2000, *ApJ*, 539, L13
 Goto, T. 2006, *MNRAS*, 371, 769
 Grandi, S. A. 1982, *ApJ*, 255, 25
 Gunn, J. E. & Peterson, B. A. 1965, *ApJ*, 142, 1633
 Haiman, Z. & Cen, R. 2002, *ApJ*, 578, 702
 Haiman, Z. & Loeb, A. 2001, *ApJ*, 552, 459
 Hennawi, J. F. & Prochaska, J. X. 2007, *ApJ*, 655, 735
 Hewett, P. C. & Foltz, C. B. 2003, *AJ*, 125, 1784
 Hogg, D. W. 1999, *ArXiv Astrophysics e-prints*
 Iwamuro, F., Kimura, M., Eto, S., Maihara, T., Motohara, K., Yoshii, Y., & Doi, M. 2004, *ApJ*, 614, 69
 Iwamuro, F., Motohara, K., Maihara, T., Kimura, M., Yoshii, Y., & Doi, M. 2002, *ApJ*, 565, 63
 Jiang, L., et al. 2006, *AJ*, 132, 2127
 Kaspi, S., Brandt, W. N., Maoz, D., Netzer, H., Schneider, D. P., & Shemmer, O. 2007, *ApJ*, 659, 997
 Kaspi, S., Smith, P. S., Netzer, H., Maoz, D., Jannuzi, B. T., & Giveon, U. 2000, *ApJ*, 533, 631
 Kobayashi, N., Tsujimoto, T., & Minowa, Y. 2005, in *Science with Adaptive Optics*, ed. W. Brandner & M. E. Kasper, 352
 Maiolino, R., et al. 2005, *A&A*, 440, L51
 Maiolino, R., Juarez, Y., Mujica, R., Nagar, N. M., & Oliva, E. 2003, *ApJ*, 596, L155
 Maiolino, R., Mannucci, F., Baffa, C., Gennari, S., & Oliva, E. 2001, *A&A*, 372, L5
 Maiolino, R., Oliva, E., Ghinassi, F., Pedani, M., Mannucci, F., Mujica, R., & Juarez, Y. 2004a, *A&A*, 420, 889
 Maiolino, R., Schneider, R., Oliva, E., Bianchi, S., Ferrara, A., Mannucci, F., Pedani, M., & Roca Sogorb, M. 2004b, *Nature*, 431, 533
 Margon, B. & Ostriker, J. P. 1973, *ApJ*, 186, 91
 Maselli, A., Gallerani, S., Ferrara, A., & Choudhury, T. R. 2007, *MNRAS*, 376, L34
 Matteucci, F. & Recchi, S. 2001, *ApJ*, 558, 351
 McGreer, I. D., Becker, R. H., Helfand, D. J., & White, R. L. 2006, *ApJ*, 652, 157
 McLure, R. J. & Dunlop, J. S. 2004, *MNRAS*, 352, 1390
 McLure, R. J. & Jarvis, M. J. 2002, *MNRAS*, 337, 109
 Meiksin, A. 2005, *MNRAS*, 356, 596
 Moorwood, A., et al. 1998, *The Messenger*, 94, 7
 Page, L., et al. 2007, *ApJS*, 170, 335
 Pentericci, L., et al. 2002, *AJ*, 123, 2151
 Pentericci, L., et al. 2003, *A&A*, 410, 75
 Peterson, B. M., et al. 2004, *ApJ*, 613, 682
 Reichard, T. A., et al. 2003, *AJ*, 126, 2594
 Richards, G. T., et al. 2002a, *AJ*, 123, 2945
 Richards, G. T., et al. 2006a, *AJ*, 131, 49
 Richards, G. T., et al. 2003, *AJ*, 126, 1131
 Richards, G. T., et al. 2006b, *ApJS*, 166, 470
 Richards, G. T., et al. 2006c, *AJ*, 131, 2766
 Richards, G. T., et al. 2004, *AJ*, 127, 1305
 Richards, G. T., Vanden Berk, D. E., Reichard, T. A., Hall, P. B., Schneider, D. P., SubbaRao, M., Thakar, A. R., & York, D. G. 2002b, *AJ*, 124, 1
 Ryan-Weber, E. V., Pettini, M., & Madau, P. 2006, *MNRAS*, 371, L78
 Salpeter, E. E. 1964, *ApJ*, 140, 796
 Schneider, D. P., et al. 2005, *AJ*, 130, 367
 Schödel, R., Ott, T., Genzel, R., Eckart, A., Mouawad, N., & Alexander, T. 2003, *ApJ*, 596, 1015
 Shen, Y., et al. 2007, *AJ*, 133, 2222
 Sigut, T. A. A. & Pradhan, A. K. 2003, *ApJS*, 145, 15
 Simcoe, R. A. 2006, *ApJ*, 653, 977
 Stern, D., Hall, P. B., Barrientos, L. F., Bunker, A. J., Elston, R., Ledlow, M. J., Raines, S. N., & Willis, J. 2003, *ApJ*, 596, L39
 Telfer, R. C., Zheng, W., Kriss, G. A., & Davidsen, A. F. 2002, *ApJ*, 565, 773
 Thompson, K. L., Hill, G. J., & Elston, R. 1999, *ApJ*, 515, 487
 Tremaine, S., et al. 2002, *ApJ*, 574, 740
 Vanden Berk, D. E., et al. 2001, *AJ*, 122, 549
 Venemans, B. P., McMahon, R. G., Warren, S. J., Gonzalez-Solares, E. A., Hewett, P. C., Mortlock, D. J., Dye, S., & Sharp, R. G. 2007, *MNRAS*, 376, L76
 Verner, E. M., Verner, D. A., Korista, K. T., Ferguson, J. W., Hamann, F., & Ferland, G. J. 1999, *ApJS*, 120, 101
 Vestergaard, M. & Peterson, B. M. 2006, *ApJ*, 641, 689
 Vestergaard, M. & Wilkes, B. J. 2001, *ApJS*, 134, 1
 Walter, F., et al. 2003, *Nature*, 424, 406
 Walter, F., Carilli, C., Bertoldi, F., Menten, K., Cox, P., Lo, K. Y., Fan, X., & Strauss, M. A. 2004, *ApJ*, 615, L17
 Wandel, A., Peterson, B. M., & Malkan, M. A. 1999, *ApJ*, 526, 579
 Wang, R., et al. 2007, *AJ*, 134, 617
 White, R. L., Becker, R. H., Fan, X., & Strauss, M. A. 2003, *AJ*, 126, 1
 Willott, C. J., McLure, R. J., & Jarvis, M. J. 2003, *ApJ*, 587, L15
 Wills, B. J., Netzer, H., & Wills, D. 1985, *ApJ*, 288, 94
 Woo, J.-H., Treu, T., Malkan, M. A., & Blandford, R. D. 2006, *ApJ*, 645, 900
 Wyithe, J. S. B., Loeb, A., & Carilli, C. 2005, *ApJ*, 628, 575
 York, D. G., et al. 2000, *AJ*, 120, 1579
 Yoshii, Y., Tsujimoto, T., & Kawara, K. 1998, *ApJ*, 507, L113